Pre-Print Manuscript:
Zhang, Z., F. Deng, Y. Huang, and R. Bridgelall, "Road Roughness Evaluation Using In-Pavement Strain Sensors," Smart Materials and Structures, 24 (11), DOI:10.1088/0964-1726/24/11/115029, 115029, October 15, 2015.

Road Roughness Evaluation Using In-Pavement Strain Sensors

Zhiming Zhang[1], Fodan Deng[1], Ying Huang[1*], and Raj Bridgelall[2]

[1]*Department of Civil and Environmental Engineering, North Dakota State University*

1340 Administration Ave., Fargo, ND 58108, USA

[2]*Upper Great Plains Transportation Institute, North Dakota State University*

1340 Administration Ave., Fargo, ND 58108, USA

ying.huang@ndsu.edu

Abstract The international roughness index (IRI) is a characterization of road roughness or ride quality that transportation agencies most often report. The prevalent method of acquiring IRI data requires instrumented vehicles and technicians with specialized training to interpret the results. The extensive labor and high cost requirements associated with the existing approaches limit data collection to at most once per year for portions of the national highway system. Agencies characterize roughness only for some secondary roads but much less frequently, such as once every five years, resulting in outdated roughness information. This research developed a real-time roughness evaluation approach that links the output of durable in-pavement strain sensors to prevailing indices that summarize road roughness. Field experiments validated the high consistency of the approach by showing that it is within 3.3% of relative IRI estimates. After their installation and calibration during road construction, the ruggedized strain sensors will report road roughness continuously. Thus, the solution will provide agencies a real-time roughness monitoring solution over the remaining service life of road assets.

1. Introduction

The United States has the largest road network in the world. The network consisted of more than 2,646,000 miles of paved roads in 2012 and it plays a significant role in the economy, defense, and mobility. The performance evaluation of such a vast network and the capacity to maintain the roadways has become increasing challenging. Roughness is a global measure of roadway serviceability that has long been one of the major criteria for road condition assessment to guide resource allocation and maintenance planning. The ASTM E867 standard defines roughness as "the deviation of a surface from a true planar surface with characteristic dimensions that affect vehicle dynamics and ride quality" [1]. Pavement roughness adversely affects vehicle wear, ride quality, and transportation safety [2-5]. The higher dynamic axle loading from roughness accelerates pavement deterioration [6]. Rough roads can also increase fuel consumption by as much as 4-5 percent [7].

Researchers and organizations proposed many different roughness statistics to describe the severity of pavement roughness, however, the international roughness index (IRI) is the most widely used [8]. The IRI computation relies on a mathematical model called a quarter-car. This model simulates the response of a serially coupled damped mass-spring system to estimate the vertical motions of equivalent wheel-assembly masses. The IRI is the accumulated absolute rate difference between the simulated sprung- and unsprung mass motions per unit of distance travelled.

Another important characterization of roughness is the power spectral density (PSD). It is a mathematical representation of the spatial wavelength composition of road profiles rather than a summary index of roughness [9]. Researchers found that most pavement profiles such as road and runway surfaces have very similar PSD shapes. This observation has led to the use of coefficients that fit exponential functions to the PSD shapes as alternative summaries of roughness. Less frequently used methods also exist. These include the profile index method which is the root-mean square of a band-pass filtered road profile [10], the ride number method which is a transformation of the elevation profile per the ASTM E-1489

standard [11], and the root mean square of vertical acceleration approach which is a statistical method based on the rate of the grade change of the longitudinal profile [12].

Roughness measuring methods fall into three major classes [13]. Class I uses the traditional longitudinal surveys by rod and level or by some other laborsaving apparatus that requires walking along the test path. The Class II techniques measure the road profile with various types of profilometers such as the Chloe-type rolling straightedge [13]. Class III is an indirect measuring method described as a response-type road roughness meters (RTRRM) that most highway agencies used until the mid-1980s or as an inertial road profilers that began in the 1960s [14]. The RTRRM devices measure the response of the vehicle to the road profile using transducers to accumulate the vertical movement of the axle with respect to the vehicle's body. This method directly reflected the users' ride quality experience. However, variations in suspension characteristics and speed result in measurement inconsistencies. Such approaches also do not provide a sample of the pavement longitudinal profile for spectral analysis.

The inertial road profiling methods use instrumented vehicles to collect road roughness data [15]. Inertial profilers collect pavement condition data at highway speeds and record sufficient data to evaluate the spectral content of the pavement profile. This benefit has led to a substantial increase of countries adopting the method. The principal components of a high-speed profiler include laser-based height sensors, accelerometers and an accurate distance measuring system. The height sensors record the distance from the base of the vehicle to the pavement surface. Accelerometers above the height sensors record the vertical acceleration of the sensor to correct for reference plane bounces. In theory, double integration of the vertical acceleration signal would recover the vertical displacement of the vehicle. Practically, however, noise and initial conditions tend to create additional issues that limit their use in urban and local roads where the profiling vehicle must travel at low speeds and accommodate stop-and-go conditions [16]. Nevertheless, in more ideal settings such as freeways, the inertial profiler equipment produces a longitudinal profile of the pavement from the two height measurements. In addition to the profilers, more cost-effective approaches

are evolving based on participatory sensing methods and the use of accelerometers and geospatial position sensors aboard connected vehicles [17, 18].

Although reports (NCHRP Report 334) indicate that most agencies now use inertial profilers [17], the literature has very little information about their cost to acquire, operate, and maintain. One study reported the contracted pavement profile data collection and analysis costs ranged from $2.23/mile to $10.00/mile, with an average of $6.12/mile [18]. However, the reported costs did not include overhead such contract administration, equipment maintenance, and equipment depreciation. In general, the relatively high expense and labor requirements of existing approaches prevent agencies from monitoring large portions of their roadway network more often than once annually. Thus, they often make maintenance and rehabilitation decisions based on outdated roughness data. In addition, infrequent roughness measurements preclude the identification of dangerous distress symptoms such as frost heaves that appear and disappear between annual monitoring cycles. These situations result in roadway safety gaps that increase liability.

In addition to the roughness measurements, many agencies developed models to predict road performance using measured distress information for both flexible and rigid pavements. The distress information includes strain data, cracking condition, spalling, pop out, scaling, and a variety of other visible symptoms. The AASHTO and FHWA successfully modeled roughness indices such as the IRI or present serviceability rating (PSR) using key pavement distress information [19-23]. Among various models, empirical and mechanistic analysis have identified several pavement design features and site conditions including the pavement's temperature, moisture, and axle load cycles that affect the roughness of flexible pavements [19, 24, 25]. NCHRP developed the prediction models for rigid pavements by assembling all the available distress databases [26, 27] and considering their initial IRI. Though many of those factors are a result of pavement strains, none of the previous studies related the IRI directly to the strain distribution inside pavements by mechanistic analysis alone, without using statistical models. Such mechanistic-empirical models provide a prediction of the roughness progression but not a direct measure of the actual roughness.

Agencies require a direct measure of the actual pavement roughness as the pavement ages to guide effective maintenance and rehabilitation decisions. Therefore, this paper introduces an approach to evaluate and report the real-time pavement roughness by linking the output of in-pavement strain sensors to the IRI and other roughness indices. This method requires initial installation of the durable strain sensors inside the pavements. During road operation, the sensors report strain data that indicates the level of structural deterioration. The method developed in this study will subsequently produce the IRI by relating the vertical displacement of the pavement to the strain data. An ability to recover the elevation profile using this method also provides a generalized approach for linking it to other summary roughness indices. After installation and calibration, the sensors will provide real-time roughness monitoring continuously, throughout the remaining service life of the pavement assets. Therefore, the agencies evaluate the pavement roughness at any time.

The organization of the remaining paper is as follows: Section 2 develops the theoretical method that quantifies the road unevenness by using the output of the in-pavement strain sensors. Section 3 conducts a sensitivity study of the sensor deployment intervals and the noise levels of their output. Section 4 validates the reliability of this method using data from the field tests. Finally, Section 5 provides the conclusion and outlines the potential future work.

2. Theoretical Analysis

Roughness occasionally exists as part of the roadway design or construction defects [28], and pavement wear increases the roughness levels over time since a deformation of the pavement structure would produce a change in the road profile. Consequently, a deformation-induced increase of strain within the pavement structure must correspond to an accumulation of profile unevenness. This section first derives the theoretical relationship between the roughness condition and the accumulated strain distribution within the pavement structure along a concrete-paved road, then describes a procedure for the IRI calculation. Finally, the section introduces the previously developed connected vehicle method of roughness evaluation that the experimental study will use for validation.

2.1 Theoretical Relationship between In-pavement Strains and Roughness for Concrete-paved Roads

This paper uses concrete pavements for the theoretical analysis. The analysis for other types of roads will follow similar procedures. The deformation of concrete pavement slabs commonly uses an assumption of a thin plate panel for theoretical modelling to simplify the analysis from 3-dimensions (3-D) to 2-dimensions (2-D). According to the Kirchhoff–Love plate theory [29], the strain in the longitudinal (x) direction of a thin-plate concrete panel, ε_x, located inside the pavement at some known vertical position h_0, is expressed as:

$$\varepsilon_x = -h_0 \frac{\mathrm{d}^2 w}{\mathrm{d}x^2}, \tag{1}$$

where w is the vertical displacement of the concrete pavement panel which is also known as the road elevation profile. With the sampling interval requirement satisfied, double integration of Equation (1) reproduces the relation between the road elevation profile and the measured strains from the in-pavement sensors as:

$$w = -\iint \frac{\varepsilon_x}{h_0} \mathrm{d}x. \tag{2}$$

The IRI then becomes available because the slope rate of the road profile, $\ddot{w}$, which is the second derivative of the elevation profile, w, with respect to time, is a direct input to the procedure that computes the IRI. For a temporal road profile of ξ, the second derivative with respect to time is

$$\ddot{\xi} = -\ddot{w} = \frac{v^2 \varepsilon_x}{h_0} \tag{3}$$

where v = 80 km/h is the IRI standard speed [8].

2.2 IRI Calculation Based on In-pavement Strains

The Highway Safety Research Institute (HSRI) defines the IRI in terms of the responses from a standard quarter-car model having two degrees of freedom as shown in Figure 1.

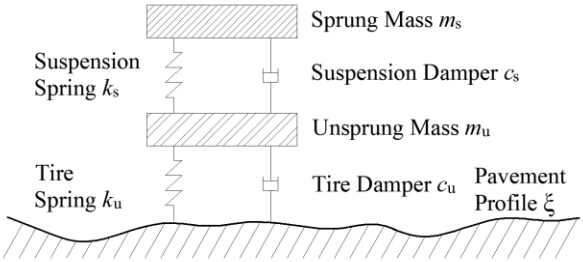

Figure 1. The HSRI Quarter-car Model.

The parameters y^t_s and y^t_u are absolute displacements of the sprung- and unsprung-mass, respectively. The HSRI quarter-car parameters are k_u/m_s = 653.0 s^{-2}, k_s/m_s = 63.3 s^{-2}, m_u/m_s = 0.15, c_s/m_s = 6.0 s^{-1} and c_u/m_s = 0.0 s^{-1}. Let the relative displacement of sprung mass be y_s and that of the unsprung mass be y_u such that

$$y_s = y^t_s - y^t_u \quad \text{and} \quad y_u = y^t_u - \xi. \tag{4}$$

Expressed in matrix-form, the ordinary differential equations to define the system dynamics for the sprung and unsprung mass is

$$M\ddot{Y}(t) + C\dot{Y}(t) + KY(t) = R(t) \tag{5}$$

where

$$M = \begin{bmatrix} m_s & m_s \\ 0 & m_u \end{bmatrix}, C = \begin{bmatrix} c_s & 0 \\ -c_s & c_u \end{bmatrix}, K = \begin{bmatrix} k_s & 0 \\ -k_s & k_u \end{bmatrix},$$

$$\ddot{Y} = \begin{Bmatrix} \ddot{y}_s \\ \ddot{y}_u \end{Bmatrix}, \dot{Y} = \begin{Bmatrix} \dot{y}_s \\ \dot{y}_u \end{Bmatrix}, Y = \begin{Bmatrix} y_s \\ y_u \end{Bmatrix}, \text{ and } R = \begin{Bmatrix} -m_s \ddot{\xi} \\ -m_u \ddot{\xi} \end{Bmatrix}$$

Substituting Equation (3) into the expression for R provides

$$R = \begin{Bmatrix} -m_s \dfrac{v^2 \varepsilon_x}{h_0} \\ -m_u \dfrac{v^2 \varepsilon_x}{h_0} \end{Bmatrix} \tag{6}$$

Solving Equation (5) with a numerical algorithm such as the Newmark method yields the relative displacements y_s and y_u, the relative velocities $\dot{y}_s$ and $\dot{y}_u$, and the relative accelerations $\ddot{y}_s$ and $\ddot{y}_u$ as a function of the in-pavement strains and velocities of the vehicle. The IRI is then [8]:

$$\text{IRI} = \frac{1}{L}\int_0^T |\dot{y}_s| \mathrm{d}t \tag{7}$$

in which, L is the segment length and $T = L/v$ is the travel time. For a computational sample interval of Δt, the number of intervals is $n = T/\Delta t$ and the discrete-time form of the computation becomes

$$\text{IRI} = \frac{1}{vn\Delta t}\sum_{i=0}^{n} |\dot{y}_s(t_i)|\Delta t = \frac{1}{vn}\sum_{i=0}^{n} |\dot{y}_s(t_i)| \tag{8}$$

2.3 Connected-Vehicle Method for Roughness Evaluation

Although the IRI is very commonly applied, the current practice of computing the IRI from elevation profile measurements using laser profiler or similar apparatus requires specific instrumented vehicles to perform the measurements. The relatively high cost for calibrated instruments and specialized expertise needed to produce the IRI limit its potential for widespread use. Connected vehicles, thus, present an opportunity to measure the roughness of the pavements more cost-effectively and conveniently by analyzing data from vehicle-integrated inertial and geospatial position sensors. Such sensors are available in most smart phones. Bridgelall [30] introduced the road impact factor (RIF) transform to summarize road roughness in direct proportion to the IRI. The RIF-index is

$$R_{\bar{v}}^{L} = \sqrt{\frac{1}{L}\int_0^{L/\bar{v}} |g_z(t)v(t)|^2 \mathrm{d}t} \tag{9}$$

where $g_z(t)$ is the resultant vertical acceleration from the inertial sensor mounted on vehicle, $v(t)$ is the instantaneous vehicle speed at time t, $\bar{v}$ is the average speed, and L is the traversal path distances for each consecutive segment analyzed.

The RIF-transform summarizes roughness in units of g-force per meter. It isolates the average ride roughness induced primarily from road unevenness, without including the impacts from other factors such

as driver behavior and vehicle handling. Applications that need to include those other factors integrate roughness from the lateral and longitudinal accelerations using a similar model [31]. The Ensemble Average RIF (EAR) is the average of RIF-indices from a predetermined speed band. The EAR-index represents the average roughness from road unevenness that riders experienced when traveling the segment at the average speed indicated. The speed range of a typical speed band is ±5 mph about the average speed indicated. Previous studies demonstrated theoretically and experimentally that the EAR-index and the IRI are directly proportional [17]. Therefore, the EAR-index can extend models that currently use the IRI by calibrating them with a constant of proportionality.

3. Sensitivity Study

This section conducts the sensitivity study of the roughness evaluation process displayed in Section 2. The factors influencing the accuracy of the IRI estimation using the measurements from in-pavement strain sensors mainly include the implementation sensor interval and the sensor signal's quality characterized by the signal-to-noise ratio (SNR). From Equation (3), it can be seen that the in-pavement strain is directly proportional to the second derivative of the profile ($\ddot{\xi}$). The interval of the road profile samples (ξ) and the second derivative of the profile ($\ddot{\xi}$) can represent the strain sensor position intervals and the output signal of the sensors, respectively.

To simulate road profiles (ξ) of different roughness levels for sensitivity analysis, the inverse fast Fourier transform (IFFT) of the PSD is a suitable approach to apply [32, 33]. For this analysis, the second-order forward difference provides a higher-accuracy numerical approximation of the second derivative of the profile ($\ddot{\xi}$) [34]. After solving Equation (5) using the Newmark method, Equation (8) then provides the associated IRI for the profile [34]. The variation in IRI is observable by changing the profile sampling interval size, which represents the strain sensor interval, for each evaluation of Equation (5). The method of noise sensitivity analysis involves adding white Gaussian noise to the in-pavement strains (ε_x) thus, to the profile's slope rate ($\ddot{\xi}$), and observing the IRI variations.

3.1 Roughness Generation

The ISO (1995) [35] represents the elevation profile (ξ) as a PSD such that

$$S_{\xi}(\kappa) = \begin{cases} S_{\xi}(\kappa_0)\left(\frac{\kappa}{\kappa_0}\right)^{-n_1} & \frac{\kappa}{\kappa_0} \le 1 \\ S_{\xi}(\kappa_0)\left(\frac{\kappa}{\kappa_0}\right)^{-n_2} & \frac{\kappa}{\kappa_0} > 1, \end{cases} \tag{10}$$

where, κ is the wavenumber with a unit of cycle/m, κ_0 is the datum wavenumber in cycle/m, $S_{\xi}(\kappa)$ is the road profile PSD in an unit of m^3/cycle, and $S_{\xi}(\kappa_0)$ is the PSD at κ_0 or initial PSD in m^3/cycle.

For typical profiles, Cebon [36] recommended n_1=3, n_2=2.25, and κ_0=1/(2π) cycles/m. Table 1 summarizes the qualitative relationship between the roughness classification and the initial PSD. As expected, higher values of $S_{\xi}(\kappa_0)$ corresponds to poorer road condition in terms of roughness levels.

Table 1. Relationship between roughness classification and initial PSD [36]

Roughness Classification	$S_{\xi}(\kappa_0)$ 10^{-6} m^3/cycle
Very Good	2-8
Good	8-32
Average	32-128
Poor	128-512
Very Poor	512-2048

Reference [37] indicates that the IRI does not respond to spatial wavelength components that fall outside of the 1.3 m to 30 m wavelength band. Therefore, the κ range from 0.02 cycle/m to 5 cycle/m is conservative for the IFFT computation. Figure 2a shows the road profile generated with $S_{\xi}(\kappa_0) = 3.2\times10^{-5}$ m^3/cycle, and Figure 2b shows the corresponding PSD.

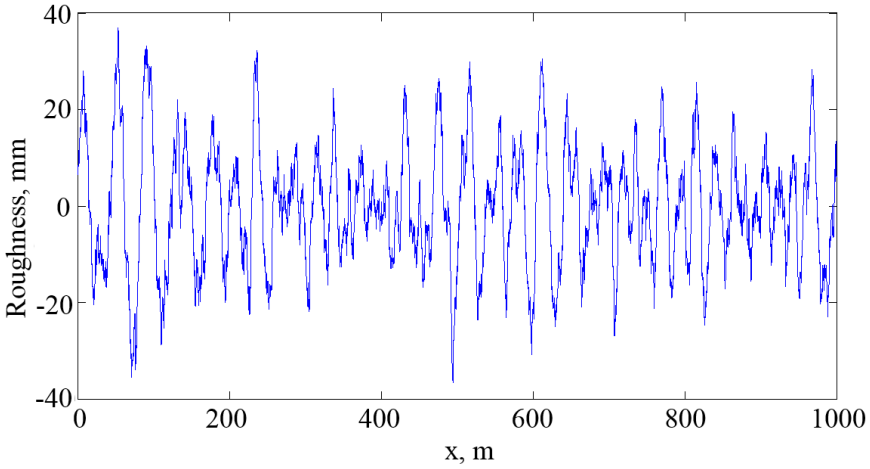

(a) Generated Road Profile

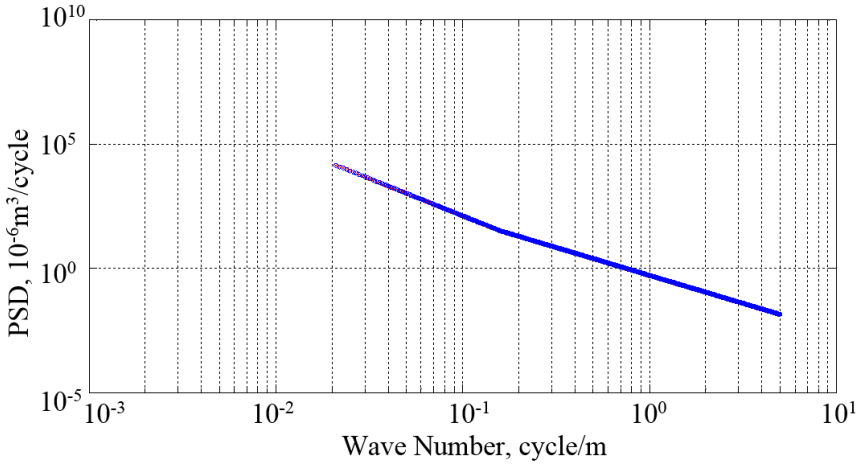

(b) Comparison on the Power Spectral Density

Figure 2. Roughness Generation at $S_\xi(\kappa_0) = 3.2\times10^{-5}$ m^3/cycle.

3.2 Sensitivity on In-pavement Strain Sensor Interval

The Nyquist-Shannon sampling theorem dictates a minimum profile sampling interval of 0.65 m because the IRI becomes insensitive to wavelengths shorter than 1.3 m. Figure 3 shows the change of IRI with the sensor interval for the roughness generated at $S_\xi(\kappa_0) = 3.2\times10^{-5}$ m^3/cycle. As shown in Figure 3, the IRI steadily decreases as sensor interval increases. The tradeoff between IRI accuracy and in-pavement strain sensor interval directly relates to the expense of sensor installation. The recommended standard sampling interval is 0.3 meters using the vehicle based profiling approaches [8]. However, installing strain sensors at the equivalent sampling intervals would require a significantly large number of strain sensors that would result in a high initial installation cost.

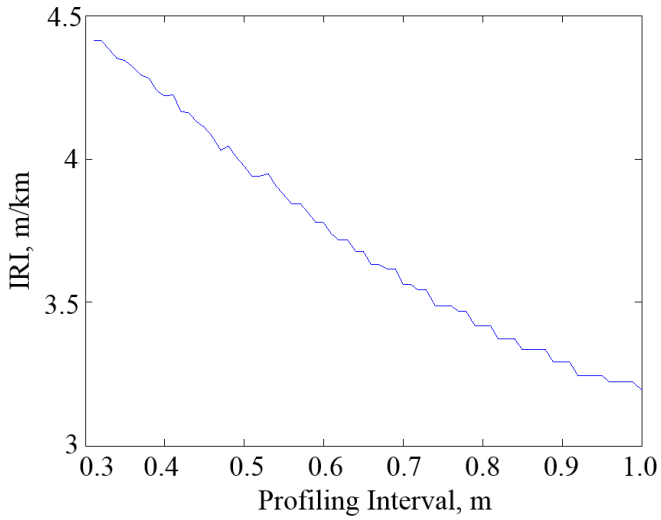

Figure 3. IRI at Different Strain Sensor Intervals

To potentially reduce the number of sensors needed for a more cost-effective solution, Table 2 compares various sensor interval compared with the IRI calculated from standard intervals of 0.3 m for different levels of roughness $S_\xi(\kappa_0)$ with measurement accuracies of 90% and 80%. The results indicate that larger IRI or rougher surfaces require fewer sensors. Since the road roughness matter more when the IRI increases, users can increase the sensor interval to decrease cost without losing measurement accuracy. A sensor interval of 0.7~0.8 m would provide an accuracy within 80% for roughness levels that correspond to the road conditions with average or below that matter most to the agencies. Hence, trading off 20% accuracy reduces the required number of in-pavement strain sensors by at least a factor of two. For specific applications, a sensor interval analysis is highly recommended before the sensor installation.

Table 2. Sensor Intervals Required for an Accuracy of 80% and 90%

$S_\xi(\kappa_0)$, 10^{-6} m^3/cycle	2	4	8	16	32	64	128	256	512	1024	2048
IRI at 0.3 m, m/km	1.12	1.57	2.23	3.19	4.55	6.33	8.92	12.76	17.95	25.04	36.14
Sensor Interval with 90% Accuracy, m	0.3	0.3	0.3	0.4	0.4	0.5	0.5	0.5	0.5	0.5	0.5
Sensor Interval with 80% Accuracy, m	0.4	0.5	0.6	0.6	0.7	0.7	0.8	0.7	0.7	0.8	0.8

3.3 Sensitivity on Sensor Signal Quality

This section uses the ASTM Standard E 1926-98 [8] profile with known IRI to study the noise sensitivity of the in-pavement strain sensor on IRI estimation. Figure 4 shows the simulated standard

sinusoidal road profile. Table 3 lists the calculated IRI values and the relative errors for different levels of white Gaussian noise. The relatively small error of 5.0% between the IRI of the ASTM profile and the IRI computed from generating the slope rate estimated from the strain-based method in this paper validates the method. Adding noise levels ranging from 3 dB to 10 dB to the slope rate of the profile estimated from the strain-based approach result in relative errors that are less than 5% as listed. This result demonstrates that the developed strain-based roughness estimation method is relatively insensitive to noise.

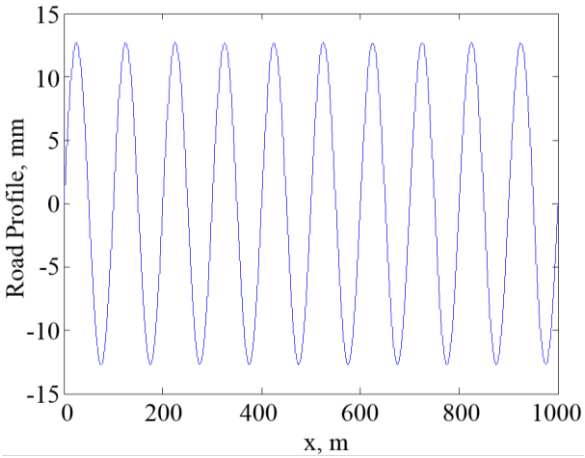

Figure 4. Road Profile (ASTM Standard E 1926-98 [8])

Table 3. Validation of the Method for IRI Calculation.

Parameter	ASTM	Strain-based Method from This Paper			
		No Noise	3 dB Noise	8 dB Noise	10 dB Noise
IRI	0.0222	0.0211	0.0226	0.0216	0.0215
Relative Error	-	5.0%	1.8%	2.7%	3.2%

4. Field Experimental Validations and Discussions

The high-resolution localization feature of the connected-vehicle method of roughness characterization provided validation for the in-pavement strain sensor method. Minnesota Department of Transportation (MnDOT) owns and operates a road section of the Cold Weather Road Research Facility in Minnesota (MnROAD) that contains various in-pavement strain sensors. MnROAD consists of two unique roadways: a two-lane low-volume loop that is loaded with a 5-axle 80,000 lb (36,287 kg) semi, and a section of interstate I-94 ‘‘mainline’’ that contains two westbound lanes with live traffic. Figure 5a shows the two roadway sections. The site for the field testing was Cell-40, which is an existing pavement test section on the low-volume road as shown in Figure 5a. Figure 5b shows the seventy concrete pavement panels selected

for roughness evaluation; they are numbered Panel 0 through Panel 69. The length of each panel is 6 ft, so the total length of test section is 420 ft. Figure 5c is a photo of the concrete panel series in Cell-40 for visual evaluation. The rest of this section describes the field tests, analyzes the results, and finally validates the strain-based method using the connected vehicle approach.

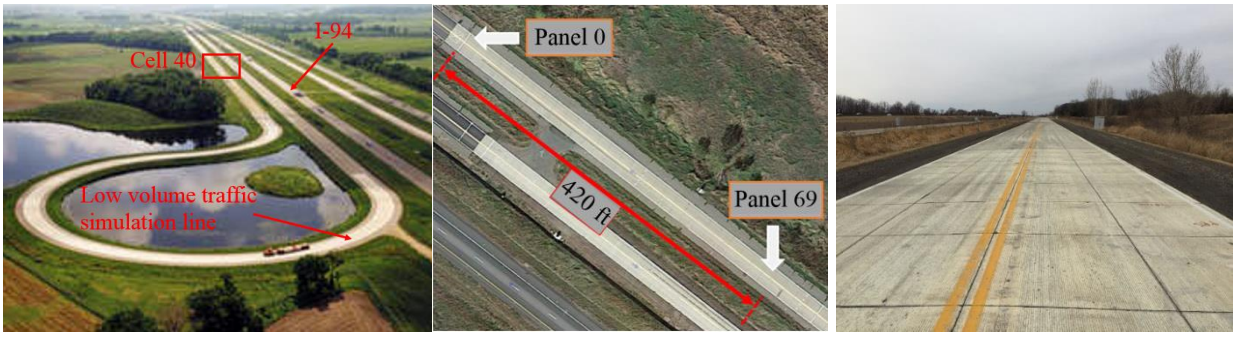

(a) Testing Facilities at MnROAD (b) Plane View of the Testing Panels (c) Photo of Cell-40

Figure 5. Road Sections at MnROAD for Roughness Evaluation

4.1 Roughness Evaluation Using the In-pavement Strain Sensors

This method measures the accumulated strains during the simulated traffic on the road section and calculates the present roughness level (IRI) using the method developed in Section 2.

4.1.1 Experimental Setup

The authors' research group previously developed multiple glass fiber reinforced polymer packaged fiber Bragg grating (GFRP-FBG) sensors and installed them within three panels of Cell 40 at MnROAD [38]. Reference [38] provides details of the sensor principle, sensor design, and installation procedures. Panels 36, 40, and 53 embedded the GFRP-FBG sensors as shown in the layout in Figure 6. The three panels contained sensors that measure strains in one dimension (1-D), and panels 36 and 40 contained one additional sensor each that can measure strains in three dimensions (3-D). The sensors were located above a 0.5-inch (13 mm) elevation level relative to the bottom surface of the pavement panel, and along the truck wheel path. The orientations of the 1-D and 3-D sensors are as indicated in the Figure 6. This experiment used only the longitudinal component of the three orthogonal sensors of the 3-D version for strain measurements. In addition, a temperature tree installed on the side of each panel provided data to compensate for environmental effects on the strain measurements.

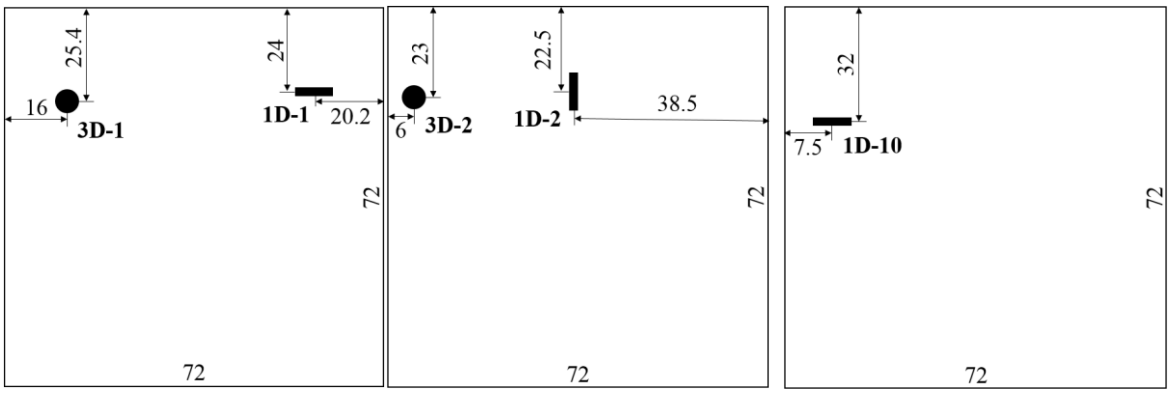

(a) Panel 36 (b) Panel 40 (c) Panel 53

Figure 6. Sensor Layout at the Pavement Panels (Unit: in.)

4.1.2 Results and Analysis

After temperature compensation, the analysis treats the strain distribution along the wheel path of each panel as step functions (Figure 7). The first transition point is equidistant to the sensor's position from the panel edge. The orientation of the 1-D sensor within Panel 40, 1D-2, is in the traverse direction. The history of the strain values from the three sensors indicates that the analysis need not differentiate between values in the longitudinal and transverse directions [39] for static strain measurements. As Panel 53 has a single sensor, there will be no transition points. The sampling intervals between strain sensor positions are 0.9 m for Panel 36, 0.7 m for Panel 40, and 1.8 m for Panel 53. Following the procedure in Section 2 for the strain-based method, the estimated IRI values are 2.00, 2.01, and 1.92 for Panel 36, Panel 40, and Panel 53, respectively. According to the sensitivity study on sensor interval performed in Section 3 and shown in Table 2, the accuracy of estimated IRI for the Panel 36 and 40 are around 80% and that for Panel 53 will be less than 80%. This is within expectations because the single sensor of Panel 53 must produce a larger error than for the other two panels that contain two sensors each that shorten the interval between samples.

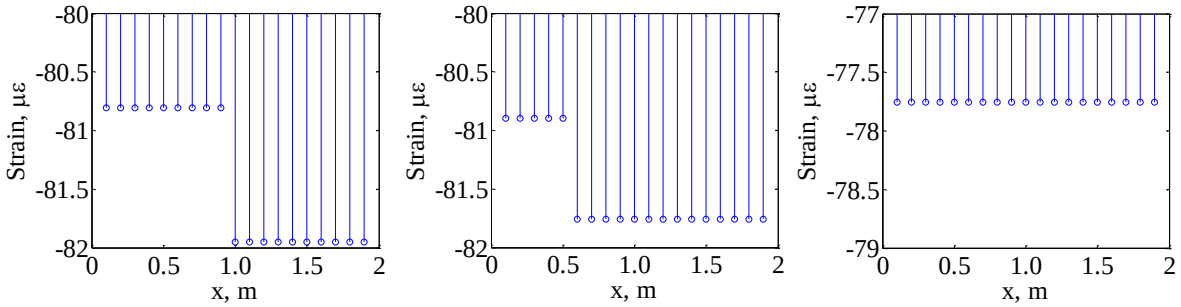

(a) Panel 36 (b) Panel 40 (c) Panel 53

Figure 7. Strain Distribution along the Wheel Path Track of Each Testing Panel

4.2 Roughness Estimation Using the Connected-Vehicle Method

Different from the strain-base method discussed above, the connected-vehicle method is a response type method that measures the vertical acceleration at a specific location of the vehicle travelling along the wheel path. The RIF-transform requires only a regular passenger vehicle and does not require the standard survey vehicle used for producing the IRI. Both roughness indices reflect the relative roughness levels of each road segment traversed [30].

4.2.1 Field Testing Using the Connected-Vehicle Approach

This study used a regular passenger vehicle, a 2011 Chevrolet Traverse as shown in Figure 8, to collect the inertial and geospatial position data needed for the RIF-transform. Three smart phones secured flat in the vehicle's rear trunk ran a data logger application (app) that logged the resultant vertical accelerations. Figure 9 shows a top view of the smartphone installation, including their orientations. Phone 1 and Phone 2 were iPhone® 4S devices fixed in the longitudinal orientation whereas Phone 3 was an iPhone® 5 oriented in the lateral direction. The GPS receiver had an update rate of 1 Hz and the accelerometer was set to sample at 128 Hz based on recommendations from prior studies [40]. The iOS® app logged inertial and geospatial position data as the vehicle traversed the 70 panels selected for roughness evaluation.

Figure 8. Passenger Vehicle for Roughness Evaluation (2011 Chevrolet Traverse)

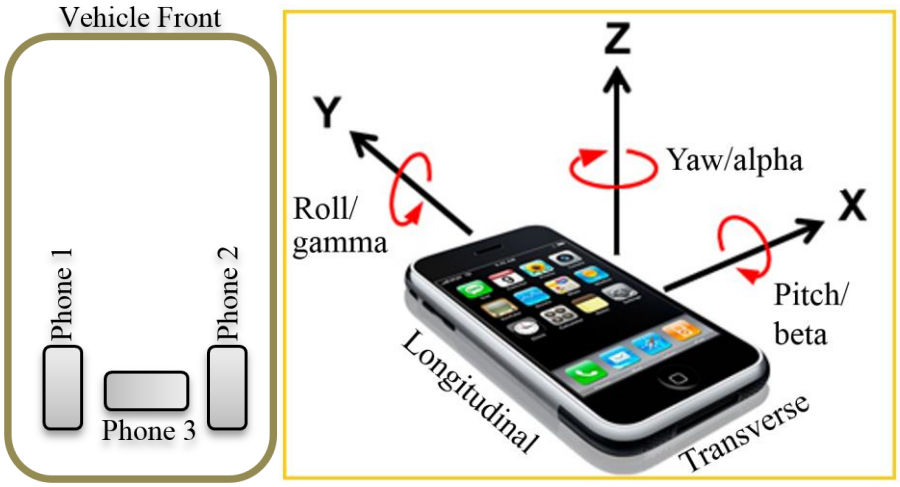

(a) Smart Phone Layout (b) Orientation of Smart Phone

Figure 9. Smart Phone Installation at the Rear Trunk for Fielding Testing

4.2.2 Testing Results and Analysis

A comma separated value (CSV) file format is the recommended organization for RIF-transform data as shown in Table 4. The first row contains a header with labels for each column of data sampled from the inertial and geospatial sensors on the smart phones. The integrated timer provides the "Time" data in milliseconds. The integrated GPS receiver provides the latitude (L_{at}) and longitude (L_{on}) data in decimal format, and the ground speed (G_{speed}) in m/s. The integrated inertial sensor provides the accelerator values for the g-forces sensed in the vertical, lateral, and longitudinal directions as "G_z", "G_x", and "G_y", respectively and normalized to 9.81 m/s^2. The integrated gyroscope produces the "Pitch," "Roll," and "Yaw" for the sensor orientation angles in degrees, respectively. After inertial sensor orientation calibration, travel distance estimation, and roughness characterization as described in [41], the calculated

RIF-indices are as displayed in Figure 10 for all the 70 panels. The EAR-index for the three panels deployed with the in-pavement strain sensors are 0.149, 0.162, and 0.144 for Panel 36, Panel 40, and Panel 53, respectively.

Table 4. Standard Data Format Used to Compute RIF

Time	L_{at}	L_{on}	G_{speed}	Pitch	Roll	Yaw	G_x	G_y	G_z
114421	45.27234	-93.6994	16.92	-0.09375	2.375	-0.0625	-0.327	-0.0335	-1.0165
114429	45.27234	-93.6994	16.92	-0.625	1.6875	1.1875	-0.334	-0.041	-1.0185
114437	45.27234	-93.6994	16.92	-0.90625	1.78125	-0.40625	-0.3315	-0.0405	-1.027
114445	45.27234	-93.6994	16.92	0.90625	1.40625	0.28125	-0.3275	-0.0405	-1.0045
114453	45.27234	-93.6994	16.92	-0.25	1.375	-0.75	-0.324	-0.0425	-0.9845
114460	45.27234	-93.6994	16.92	0.1875	0.96875	0.0625	-0.3225	-0.05	-0.9805
114468	45.27234	-93.6994	16.92	-0.125	1	0.3125	-0.335	-0.0555	-1.005

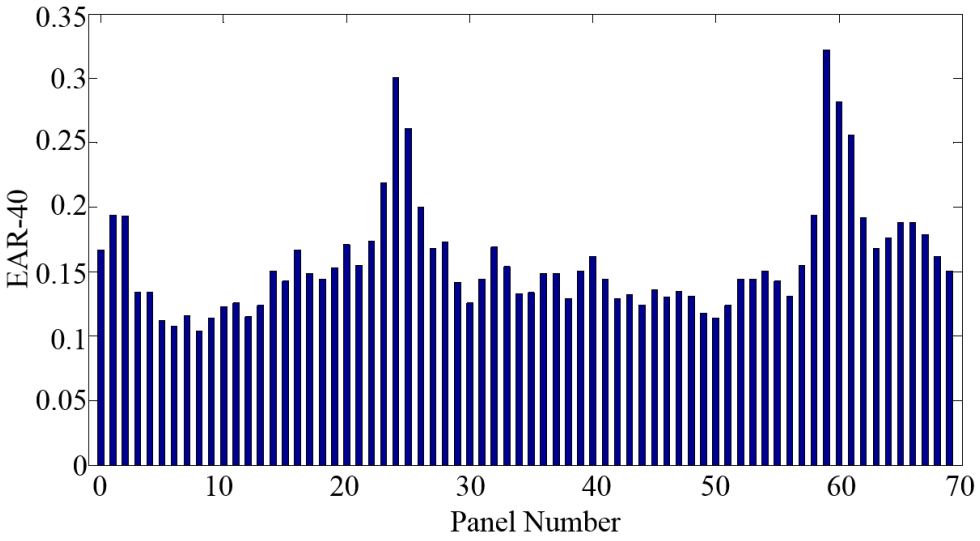

Figure 10. Estimated EAR-index for Panel 0-69 using Connected Vehicle Method

4.3 Validation of Roughness Estimation Using In-pavement Strain Sensors

The high cost of traditional methods for obtaining the IRI presents a significant barrier to validating the developed strain-based method in this paper by using a laser-based profiler vehicle. However, the direct proportionality relationship between the IRI and the EAR-index provides a cost-effective means of validating the developed roughness estimation method using in-pavement strain sensors by comparing it with the respective roughness indices obtained from the connected vehicle approach for the three panels. Table 5 compares the estimated IRI using the strain-based method and the obtained EAR-indices from the connected-vehicle method for Panel 36, Panel 40, and Panel 53 and their ratios. The ratios of the IRI to the

EAR-indices for the three panels range from approximately 12 to 14. The estimated IRI is proportional to the EAR-indices at an average ratio of 13.04, and the standard deviation of the ratios is only 3.3% of the mean. This indicates a high degree of consistency in the IRI values derived from the developed strain-based method. It demonstrates that the IRI estimated from the in-pavement strain sensors is directly proportional to the EAR-indices from the connected-vehicle method [21] as expected, and this result validates the effectiveness of the IRI evaluation using the in-pavement strain sensors.

Table 5. Comparison of IRI and EAR-index on Sensor-Deployed Panels

	Panel 36	Panel 40	Panel 53
IRI derived from strain-based method	2.00	2.01	1.92
EAR-index from the connected-vehicle method	0.149	0.162	0.144
IRI/EAR-index	13.40	12.43	13.31

5. Conclusions and Future Work

This paper provides transportation researchers and engineers with a cost-effective method of road roughness evaluation using strain sensors deployed inside the pavement. The authors conducted theoretical and numerical analysis to develop the relation between the measured strains from the in-pavement strain sensors and the IRI, followed by field experiments to validate the theoretical development. The conclusions of this paper are as follows:

1) The strain series that develop gradually and accumulate with road use is directly proportional to the second derivative of the road elevation profile. The procedure that produces the IRI is a linear time-invariant transformation of the second derivative of the road elevation profile. Therefore, the IRI is directly proportional to the strain data.

2) Numerical simulation proves that a measurement accuracy of 80% or higher is achievable using the strain-based method at a specific sensor implementation interval of 0.7 m or shorter for the roughness levels that are of most concern to agencies; the strain-based method is relatively insensitive to the noise disturbances.

3) The case studies using strain sensor data collected from three concrete panels in the field at MnROAD, MN, validated the new roughness evaluation method based on the in-pavement strain

sensors by comparing the consistency of its proportionality with a connected-vehicle method of roughness characterization that is directly proportional to the IRI.

The results of this research provide an alternative method of roughness evaluation that does not require probe vehicles. This new method will provide roadway agencies with the ability to evaluate roughness in real time and continuously throughout the service life of the road to enable improved methods of predictive asset management, and the potential for significant lifetime cost savings. Future work will apply this method to asphalt pavements and develop an integral system for road condition monitoring and traffic data collection.

6. Acknowledgement

A USDOT UTC grant under MPC agreement DTRT12-G-UTC08 provided funding for this study. The findings and opinions expressed in this article are those of the authors only and do not necessarily reflect the views of the sponsors. The authors also would like to thank Robert Strommen, Leonard Palek, Benjamin Worel, and other technicians at MnROAD facility, MnDOT, MN, for their extensive technical help during field tests.

Reference

1. ASTM, *E867 Standard Terminology Relating to Vehicle-Pavement Systems*, 2012, American Society for Testing Materials, ASTM.
2. Van Deusen, B.D., *Analytical techniques for designing riding quality into automotive vehicles*, 1967, SAE Technical Paper.
3. Brickman, A.D., et al., *Road Roughness Effects on Vehicle Performance*, 1972.
4. Abaynayaka, S., et al., *Tables for estimating vehicle operating costs on rural roads in developing countries.* 1976.
5. Gillespie, T. and M. Sayers, *Role of Road Roughness in Vehicle Ride.* Transportation Research Record, 1981(836).
6. Saleh, M.F., M.S. Mamlouk, and E.B. Owusu-Antwi, *Mechanistic roughness model based on vehicle-pavement interaction.* Transportation Research Record: Journal of the Transportation Research Board, 2000. **1699**(1): p. 114-120.
7. Klaubert, E.C., *Highway Effects on Vehicle Performance*, 2001.
8. ASTM, *E1926 Standard Practice for Computing International Roughness Index of Roads from Longitudinal Profile Measurements*, 2008, American Society for Testing Materials, ASTM.
9. Marcondes, J., et al., *Spectral analysis of highway pavement roughness.* Journal of transportation engineering, 1991. **117**(5): p. 540-549.
10. Smith, K., et al., *Smoothness specifications for pavements*, 1997.
11. ASTM, *E1489 Standard Practice for Computing Ride Number of Roads from Longitudinal Profile Measurements Made by an Inertial Profile Measuring Device*, 1998, American Society for Testing Materials, ASTM.

12. McKenzie, D. and M. Srinarawat, *Root Mean Square Vertical Acceleration (RMSVA) as a Basis for Mays Meter Calibration.* Center for Transportation Research, Univ. of Texas at Austin, Brazil Project Tech. Memo BR-23, 1978.
13. Huang, Y.H., *Pavement analysis and design*1993.
14. Brown, D., W. Liu, and T. Henning, *Identifying pavement deterioration by enhancing the definition of road roughness*2010.
15. Spangler, E.B. and W.J. Kelly, *GMR road profilometer-a method for measuring road profile.* Highway Research Record, 1966.
16. NCHRP, *Measuring, Characterizing, and Reporting Pavement Roughness of Low-Speed and Urban Roads*, 2013, Transportation Research Board.
17. Hyman, W.A., et al., *Improvements in data acquisition technology for maintenance management systems*1990.
18. McGhee, K.H., *Automated pavement distress collection techniques*. Vol. 334. 2004: Transportation Research Board.
19. Paterson, W., *A transferable causal model for predicting roughness progression in flexible pavements.* Transportation Research Record, 1989(1215).
20. Yu, H., et al., *Performance of concrete pavements. Volume III: Improving concrete pavement performance*, 1998.
21. Darter, M.I. and E.J. Barenberg, *Zero-Maintenance Pavement: Results of Field Studies on the Performance Requirements and Capabilities of Conventional Pavement Systems*, 1976.
22. Al-Omari, B. and M.I. Darter, *Relationships between international roughness index and present serviceability rating.* Transportation Research Record, 1994(1435).
23. Carey Jr, W. and P. Irick, *The pavement serviceability-performance concept.* Highway Research Board Bulletin, 1960(250).
24. Sebaaly, P.E., S. Lani, and A. Hand, *Performance models for flexible pavement maintenance treatments.* Transportation Research Record, 1995(1508): p. 9-21.
25. Kajner, L., M. Kurlanda, and G. Sparks, *Development of Bayesian regression model to predict hot-mix asphalt concrete overlay roughness.* Transportation Research Record: Journal of the Transportation Research Board, 1996(1539): p. 125-131.
26. Von Quintus, H., et al., *Appendix PP: Smoothness Prediction for Rigid Pavements. Guide for Mechanistic-Empirical Design of New and Rehabilitated Pavement Structures. National Cooperative Highway Research Program.* Transportation Research Board. Washington, DC, 2001.
27. Von Quintus, H., et al., *Appendix OO-1: Background and Preliminary Smoothness Prediction Models for Flexible Pavements. Guide for Mechanistic-Empirical Design of New and Rehabilitated Pavement Structures. National Cooperative Highway Research Program.* Transportation Research Board. Washington, DC, 2001.
28. Karamihas, S.M., M.A. Barnes, and R.O. Rasmussen, *Pavement surface specification for road load measurement.* 2014.
29. Timoshenko, S., S. Woinowsky-Krieger, and S. Woinowsky-Krieger, *Theory of plates and shells*. Vol. 2. 1959: McGraw-hill New York.
30. Bridgelall, R., *Connected vehicle approach for pavement roughness evaluation.* Journal of Infrastructure Systems, 2013. **20**(1).
31. Bridgelall, R., *RAILCOTS – Rolling Stock Automatic In-Situ Line-Quality, Car Operations, and Tracking System*, in *Sensors Expo & Conference*2013: Chicago, IL.
32. Jiang, C.D., et al. *Simulation of Road Roughness Based on Using IFFT Method*. in *Software Engineering (WCSE), 2012 Third World Congress on*. 2012. IEEE.
33. Wu, J.-J., *Simulation of rough surfaces with FFT.* Tribology International, 2000. **33**(1): p. 47-58.
34. Bender, C.M. and S.A. Orszag, *Advanced mathematical methods for scientists and engineers I: Asymptotic methods and perturbation theory*. Vol. 1. 1999: Springer.
35. Andren, P., *Power spectral density approximations of longitudinal road profiles.* International Journal of Vehicle Design, 2006. **40**(1): p. 2-14.
36. Cebon, D., *Handbook of vehicle-road interaction*1999.
37. Sayers, M.W. and S.M. Karamihas, *The little book of profiling.* Ann Arbor: Transportation Research Institute, University of Michigan., 1998.
38. Zhou, Z., et al., *Optical fiber Bragg grating sensor assembly for 3D strain monitoring and its case study in highway pavement.* Mechanical Systems and Signal Processing, 2012. **28**: p. 36-49.

39. Zhang, Z., et al., *Glass fiber–reinforced polymer–packaged fiber Bragg grating sensors for ultra-thin unbonded concrete overlay monitoring.* Structural Health Monitoring, 2015. **14**(1): p. 110-123.
40. Bridgelall, R., *Inertial Sensor Sample Rate Selection for Ride Quality Measures.* Journal of Infrastructure Systems, 2014.
41. Bridgelall, R. *A participatory sensing approach to characterize ride quality*. in *SPIE Smart Structures and Materials+ Nondestructive Evaluation and Health Monitoring*. 2014. International Society for Optics and Photonics.